InN dielectric function from the midinfrared to the ultraviolet range

A. Kasic,* E. Valcheva, and B. Monemar
Department of Physics and Measurement Technology, Linköping University, S-581 83 Linköping, Sweden

H. Lu and W. J. Schaff
Department of Electrical and Computer Engineering, Cornell University, Ithaca, New York 14853
(Received 28 February 2004; revised manuscript received 6 July 2004; published 30 September 2004)

We present a comprehensive study of the InN dielectric function from the midinfrared range up to 6.5 eV employing spectroscopic ellipsometry at room temperature. The single-crystalline InN films with Hall concentrations varying between 7.7×10^{17} and 1.4×10^{19} cm^{-3} were grown by molecular-beam epitaxy on sapphire substrates and show high structural quality. Free-carrier and phonon properties are determined precisely. The onset of the absorption edge reveals a distinct blueshift with increasing free-electron concentration, from 0.65 eV for the highest resistive material up to 0.80 eV. In the ultraviolet region, electronic interband transitions are detected at 4.84, 5.41, 5.59, and 6.10 eV, the second being the dominating one, and tentatively assigned in the Brillouin zone.

DOI: 10.1103/PhysRevB.70.115217 PACS number(s): 78.20.Ci, 78.30.Fs, 71.20.Nr, 77.84.Bw

I. INTRODUCTION

Recently, InN has attracted considerable attention due to the repeated observation of an effective band gap in the range around 0.7 eV by optical techniques,[1–5] in contrary to the long-time established value of ~1.9 eV.[6,7] From a technological point of view, the smaller band gap value would extend the possible emission range of optoelectronic devices based on III-nitrides from the deep-UV down to the near-IR region, i.e., a remarkably wide continuous spectral range would be covered using a single material class by appropriate alloying. High oxygen contents in polycrystalline films have been suggested as being responsible for a higher band gap,[8,9] while In-excess has been quoted for causing a smaller band gap.[10,11] However, this issue is still under discussion.

Further potential applications of InN are founded on its superior transport properties compared to GaN or GaAs [for a review, see Ref. 4]. InN apparently has the smallest effective electron mass among the III-nitrides and is expected to have a large saturation velocity and an extremely high peak drift velocity at room temperature rendering InN a promising material for high-speed and high-frequency electronic devices. Preparation of a satisfactory sample quality has proven difficult, however, due to the low dissociation temperature of InN and the extremely high equilibrium vapor pressure of nitrogen. Progress has been made recently to considerably improve the crystalline quality of single-crystalline InN films revealing Hall electron mobilities well above 1000 cm^2/(V s) at room temperature and background electron concentrations below 10^{18} cm^{-3}.[12] These films furthermore show intense low-temperature photoluminescence at ~0.8 eV.[5]

Fundamental physical properties of InN involving the actual band gap value and higher-energy interband transitions have yet to be elucidated. Systematic investigations of the InN dielectric function for high-quality low-absorption edge material are missing. Spectroscopic ellipsometry (SE) studies presented so far are scarce and mainly restricted to the band gap region.[13,14] Vibrational and free-carrier properties of MBE-grown InN showing a low effective band gap were recently examined using Raman scattering and mid-IR SE.[15] Additionally, some IR reflection studies have been reported recently.[16,17]

Herein, we present a comprehensive study of a series of MBE-grown InN films with free-electron concentration ranging from 7.7×10^{17} to 1.4×10^{19} cm^{-3} using SE. The data cover a wide range from 350 cm^{-1} (~43 meV) up to 6.5 eV. Phonon and free-carrier properties are obtained from the mid-IR data. The influence of the free-carrier concentration on the onset of the absorption edge is studied. Higher-energy interband transitions are detected and tentatively localized within the Brillouin zone (BZ) upon comparison to the latest results from empirical pseudopotential calculations.[18]

II. EXPERIMENT

A set of wurtzite single-crystalline InN films with varying free-electron concentrations was grown on *c*-plane sapphire substrate by molecular-beam epitaxy.[19,20] Hall-effect measurements determined the free-electron concentrations in the films ranging from 7.7×10^{17} to 1.4×10^{19} cm^{-3}. The film with the highest free-electron concentration was intentionally Si-doped, while all other films were nominally undoped. Prior to the growth of the $0.2-1.5\,\mu$m thick InN films (see Table I) with their optical axis parallel to the sample normal, undoped (GaN/) AlN buffer layers were deposited. For samples C and D, no GaN buffer layers were grown. Details on the growth process and structural characteristics of the material can be found elsewhere.[19–21] An elaborate analysis of the photoluminescence properties of films A, B, and D is given in Ref. 22.

Two different ellipsometer setups were employed for the data acquisition from the mid-IR to the UV spectral range. For the mid-IR range (350–6000 cm^{-1}), a Fourier-transform-based spectroscopic ellipsometer equipped with a rotating polarizer and a rotating compensator was used. The

TABLE I. Film thickness d, plasmon frequency ω_p, and plasmon broadening γ_p, as determined from the mid-IR SE data. The uncertainties are given in parenthesis. The free-electron concentration and mobility obtained from Hall-effect measurements are given as well.

Sample	d/ nm[a]	ω_p/ cm^{-1}	γ_p/ cm^{-1}	N_e^{Hall}/ 10^{18} cm^{-3}	μ_e^{Hall}/ $cm^2/(V\ s)$
A	1398 (12)	268 (10)	116 (33)	0.77	1340
B	929 (9)	509 (3)	110 (8)	1.7	1330
C	530 (3)	623 (3)	170 (7)	3.2	750
D	163 (2)	1052 (8)	122 (6)	6.0	600
E[b]	523 (2)	1171 (3)	115 (3)	14	800

[a]From IRSE data.
[b]Si-doped.

instrumental spectral resolution was 2 cm^{-1} in the InN reststrahlen region. In the near-IR–UV range (0.74–6.5 eV), a rotating-analyzer spectroscopic ellipsometer was utilized. The spectral resolution was 10 meV at 1 eV and ~30 meV at 5 eV. The spectra were taken at room temperature and at multiple angles of incidence between 55° and 70°. Instrumental details are reported in Ref. 23.

III. THEORY

The standard ellipsometric parameters Ψ and Δ are related to the complex reflectance ratio ρ,

$$\rho \equiv R_p/R_s = \tan\,\Psi\,\exp(i\Delta), \tag{1}$$

where R_p and R_s are the electric-field reflection coefficients for light polarized parallel (p) and perpendicular (s) to the plane of incidence, respectively.[24,25] A common representation of the ellipsometric parameters Ψ and Δ is the pseudodielectric function $\langle\varepsilon\rangle$ given by

$$\langle\varepsilon\rangle = \langle\varepsilon_1\rangle + i\langle\varepsilon_2\rangle = \sin^2\Phi\left[1+\left(\frac{1-\rho}{1+\rho}\right)^2\tan^2\Phi\right]. \tag{2}$$

Φ denotes the angle of incidence.

From the mid-IR to the UV spectral range, the experimental SE data were analyzed using multi-layer models α-InN/(α-GaN/) α-AlN/α-Al_2O_3 involving parametrized dielectric functions. The phonon and free-carrier contributions to the anisotropic dielectric function $\varepsilon_j(\omega)$ (for the electric field along $j=$ "$\perp$", "$\parallel$" with respect to the optical axis) in the mid-IR range (350–1500 cm^{-1}) were described by a factorized model allowing for anharmonic coupling effects of free-carrier plasmon excitations with LO phonons.[26,27] From this, particularly the frequency and broadening parameters of both the E_1(TO) phonon mode and the free-carrier plasmon can be determined by the data analysis. Employing the same model approach for the buffer layer materials AlN and GaN, none of the buffer layers showed significant free-carrier effects. The sapphire dielectric function was taken from Ref. 28.

In the near-IR-VIS (0.5–2.0 eV) as well as in the UV (4.0–6.5 eV) spectral range, the InN dielectric function was parameterized using a well-established critical point (CP) model dielectric function (MDF) approach.[29–31] Within this MDF approach the contribution of each CP C_i to the InN dielectric function is described by line-shape functions

$$C_i(A_i,E_i,\gamma_i,\Phi_i,n_i) = A_i\,\exp(i\Phi_i)(E_i - E - i\gamma_i)^{n_i}. \tag{3}$$

The parameters E_i, γ_i, and A_i denote the transition energy, the Lorentzian broadening, and the magnitude of the CP structure, respectively. The phase angle Φ_i is related to the amount of mixture of two adjacent CP's. Within the standard CP model, the exponent n_i is related to the dimension δ of the van Hove singularity corresponding to the CP: $n_i=\delta/2-1$.

In the near-IR-VIS range, the InN dispersion was described by one CP term ($i=0$). We employed a modification of the CP model approach, where n_0 is treated as an adjustable parameter.[32] Contributions of electronic transitions from spectral regions above the near-IR-VIS range to the MDF were considered by a pole term $A_p/({E_p}^2-E^2)$. For sample A, two Lorentzian oscillators were additionally required for the parametrization of the near-IR-VIS dielectric function in order to sufficiently model the experimental data. This may reflect spatial inhomogeneities in the 1.4μm thick InN layer being effectively mimicked by these two oscillators. For the sample with the intentionally Si-doped InN layer (sample E), a ~8 nm thick surface layer showing an E_0 value ~40 meV below the bulk E_0 value was introduced into the layer model thereby considerably improving the data description. Such a layer is most likely to be assigned to structural inhomogeneities, while the existence of a thin carrier-depleted surface layer[33] can be excluded from the mid-IR data analysis of sample E.[34] As all films were oriented with their c-axis perpendicular to the sample surface, the measurements performed at 60° and 70° angle of incidence mostly sense the dielectric function component perpendicular to the c axis, $\varepsilon_\perp$. Due to this small sensitivity to possible sample anisotropy, the material was treated as being isotropic, and thus an effective dielectric function was obtained in the near-IR-UV range. We note, however, that recent theoretical calculations revealed a noticeable anisotropy of the InN dielectric function, mainly giving rise to different amplitudes of the individual spectral features for $\varepsilon_\perp$ and $\varepsilon_\parallel$.[35] The anisotropic dielectric functions of the sapphire substrate, the AlN and GaN buffer layers were taken from Refs. 36 and 37, respectively, and were extrapolated down to 0.5 eV.

In the UV range, consideration of four CP's terms according to Eq. (1) provides an excellent description of the experimental data. Since the dimensionality of these CP's cannot be established unambiguously (see Sec. IV), all four CP's were treated to be one-dimensional, corresponding to $n_i=-0.5$ for $i=1,\ldots,4$. Again, contributions of higher-energy electronic transitions to the MDF were considered by a pole term. A top layer with optical constants, that were calculated using a Bruggeman-type effective-medium approximation of 50% void and 50% InN, considered surface-roughness effects. For the mid-IR spectral range, surface-roughness effects are negligible due to the large probing wavelengths, and were thus considered in the near-IR to UV spectral range only. The thickness of the surface-roughness layer ob-

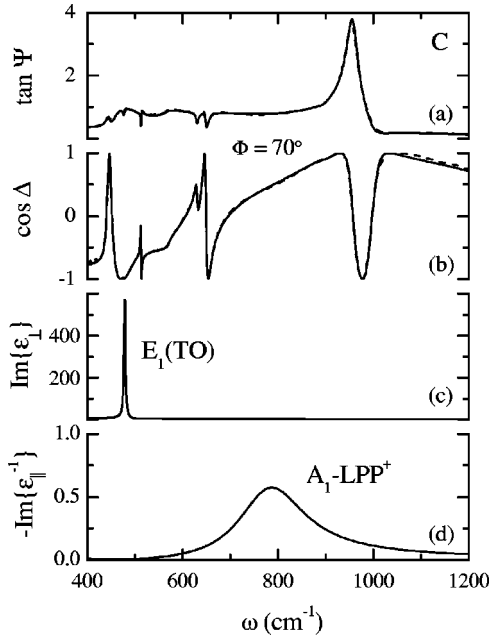

FIG. 1. (a, b) Measured (dashed lines) and modeled (solid lines) $\tan(\Psi)$ and $\cos(\Delta)$ spectra at 70° angle of incidence for sample C. (c, d) $\mathrm{Im}\{\varepsilon_\perp\}$ and $-\mathrm{Im}\{\varepsilon_\parallel^{-1}\}$ spectra, showing the E_1(TO) phonon mode and the upper LPP coupled mode branch of A_1 symmetry.

tained from the SE data analysis in the UV spectral region ranges between 3 and 14 nm within the sample series, in good agreement with results from atomic force microscopy studies.

More details on technical aspects of the SE data analysis can be found elsewhere.[15,26,38]

IV. RESULTS AND DISCUSSION

The mid-IR dielectric sample response carries valuable information on the phonon and free-carrier properties of the InN films. Figure 1 shows as an example the ellipsometric $\tan(\Psi)$ (a) and $\cos(\Delta)$ (b) spectra of sample C in the InN reststrahlen range. Experimental and modeled data agree excellently with each other. Beside the distinct spectral signatures of the InN film, those due to the ~200 nm thick AlN buffer layer and the sapphire substrate are present. The spectral dependence of the imaginary part of $\varepsilon_\perp$ (c) and the dielectric loss function parallel to the c axis (d), as deduced from the data regression analysis, are depicted in Fig. 1 as well, where the E_1(TO) phonon and the upper branch of the coupled A_1(LO)-phonon-plasmon mode (A_1-LPP$^+$) appear as maxima, respectively. Apart from sample D, the InN E_1(TO) phonon mode was determined for all samples between 477.4 and 478.5 cm^{-1}, which is consistent with both SE results from high-quality low-energy absorption edge InN[15] and with Raman scattering and IR reflection data from high-energy absorption edge material.[39,40] Remarkably, the frequency of the E_1(TO) phonon (and those of other phonon modes as well)[8] is obviously independent of the measured effective band gap. If indeed oxygen was responsible for the large band gap discrepancies observed only, phase separation in the InN-In_2O_3 system is consistent with the observed phonon behavior. For the thinnest film (sample D), the E_1(TO) phonon mode was observed at 475.4 cm^{-1} indicating a small tensile in-plane stress, provided that the biaxial strain coefficient of this phonon is of the same sign as those for GaN and AlN. This assumption is supported by a recent study combining x-ray diffraction and mid-IR SE data taken on the same sample set.[41] Furthermore, Raman scattering data from other groups showed a qualitative strain dependence of the E_1(TO) mode being similar to those of the other binary III-nitride compounds.[42,43] The fairly high crystalline quality of all InN films studied is reflected by the comparatively small E_1(TO) phonon broadening values (1.8–4.8 cm^{-1}).[44]

The plasma frequency and broadening parameters obtained from the A_1-LPP$^+$ mode are listed in Table I for all films. As the Hall concentration values carry large uncertainty values (~±30%), the effective electron mass and its possible dependence on the free-electron concentration cannot be deduced reliably from the plasmon frequency. In order to clarify this issue, magneto-ellipsometric experiments are required, which are currently in preparation.

Spectroscopic ellipsometry in the near-IR and visible range was employed to investigate the properties of the InN films in the region of the absorption onset. Figure 2 reveals the ellipsometric spectra of all samples from 0.5 to 2.0 eV. The line shapes are strongly influenced by differences in InN film thickness and buffer layers within the sample set. In Fig. 3, the extracted dielectric functions of all InN layers are shown. The ε_2 spectra have in common a fairly blurred edge in the range ~0.65–0.85 eV accompanied by a gradual increase up to the visible range. None of the samples exhibits an additional spectral feature around 1.9 eV, the formerly accepted band gap value for InN. Note that possible unknown surface effects, like not-accounted contaminants, thin free-carrier accumulation layers, oxide films, as well as nonidealities inside the layer stack, like diffuse interfaces and free-carrier gradients, give rise to uncertainties of the absolute ε values on the order of ~1 for ε_1 and ~0.5 for ε_2 within the spectral range shown in Fig. 2, but affect the overall line shape and particularly the E_0 CP parameters to a very minor extent only. These effects are most likely to cause the (slight) deviations between experimental and modeled data, especially for sample E. We emphasize that the relative E_0 CP energy values in particular – and thus the observed dependence of E_0 on N_e (see below) – are found to be highly robust when tentatively using different modeling conditions (like considering different energy ranges for regression, inclusion of an oxide layer modeled by a Cauchy approach, or keeping the layer thickness fixed at the respective value deduced from the IR analysis). Within the MDF approach used, the absolute E_0 CP energy values are subject to variations within a range of approximately ±15 meV under the different model conditions mentioned above.

With increasing plasmon frequency, the step in the ε_2 spectrum, which corresponds to an onset of extinction, and accordingly the E_0 CP energy parameter (see Fig. 4) are subject to a distinct blueshift. Similar to our results, Wu *et al.* observed a pronounced blueshift of the absorption edge with increasing Hall concentration for MBE-grown InN films and quantitatively described this effect by the **kp** interaction

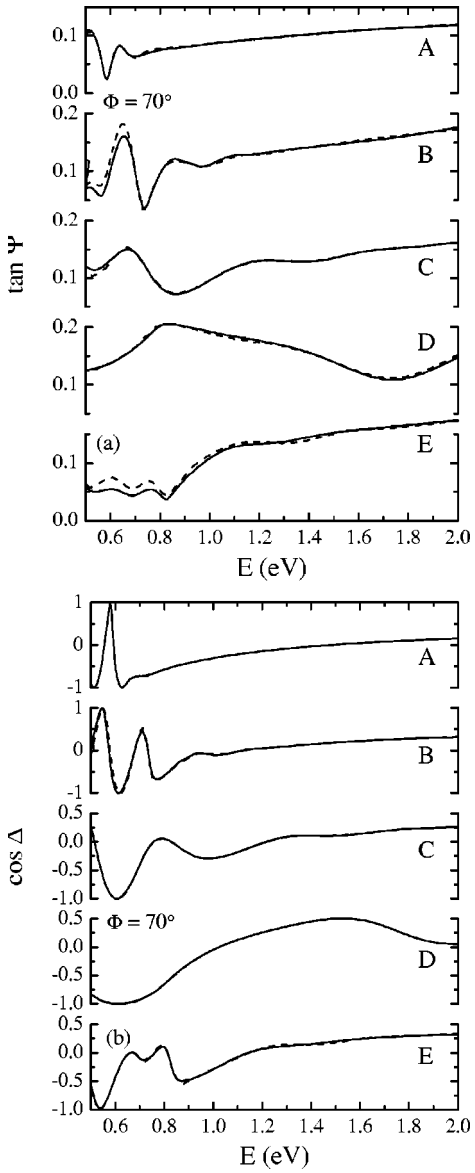

FIG. 2. Ellipsometric spectra of all samples in the near-IR and part of the visible spectral range, at 70° angle of incidence. Dashed lines, measured data; solid lines, modeled data. The differences in the oscillatory behavior of the curves in the low-energy part are partly due to different InN layer thicknesses and different buffer layers used.

within the two-band Kane model for narrow-gap material.[12] Following their approach for a non-parabolic conduction band, the observed dependence of E_0 CP energy parameter on ω_p in our sample set can be well described by considering conduction band filling (Burstein-Moss shift) and renormalization effects in terms of electron-electron and electron-ionized impurity interactions and employing realistic model parameters for the effective carrier mass, the high-frequency dielectric constant, and the interband momentum matrix element (E_p=10 eV). For the InN film of sample A with an optically determined plasmon frequency ω_p=268 cm^{-1}, equaling a free-electron concentration of N_e=3.8 $\times 10^{17}$ cm^{-3} (provided $m^*=0.07m_0$ and ε_∞=6.7),[12,15] it can be estimated that the band filling and renormalization effects

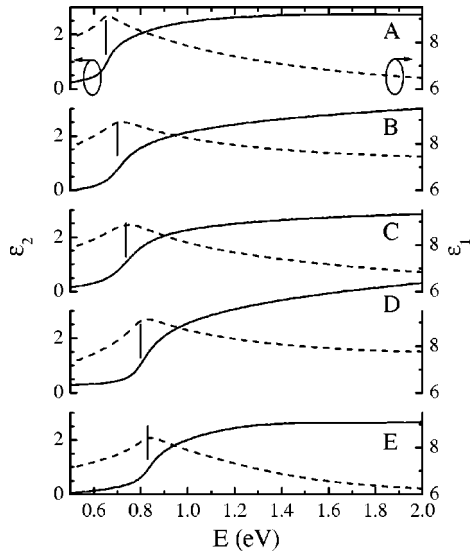

FIG. 3. Real (dashed line) and imaginary part (solid line) of the InN dielectric function for all samples, as obtained from the SE regression analysis of the data shown in Fig. 2. The blueshift of the step-like feature in ε_2 with increasing free-electron concentration is apparent. No further absorption feature is observed in the range around ~1.9 eV. The E_0 CP energies are indicated by markers.

between them cause merely an effective band gap shift of 2–4 meV. Thus, the effective band gap energy for highly resistive material, well represented by sample A, is 0.65 eV at room temperature. Nevertheless, it should be emphasized here, that the nature of the observed absorption edge cannot be assessed from the SE experiment alone, and hence it could not be excluded that alternative mechanisms involving band gap states or deviations from ideal film stoichiometry are partly responsible for the observed absorption edge below 1 eV.[10,11]

For the sake of better comparison to previously published absorption data, the squared absorption spectra inferred from the ε_2 dispersion are plotted in Fig. 5 for samples A and E.

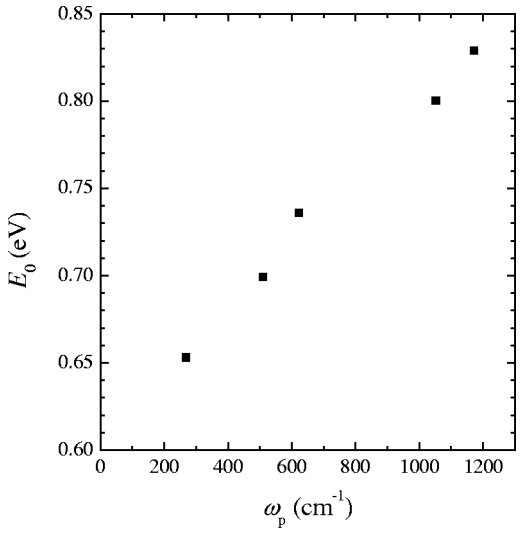

FIG. 4. E_0 CP energy parameter as a function of the plasmon frequency.

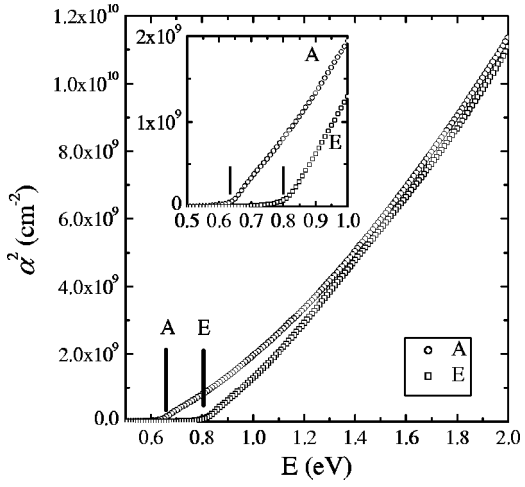

FIG. 5. Squared absorption coefficient spectra deduced from the ε_2 dispersion of the InN films of samples A and E. Vertical markers indicate the E_0 CP energies according to (3). The inset enlarges the onset of the absorption.

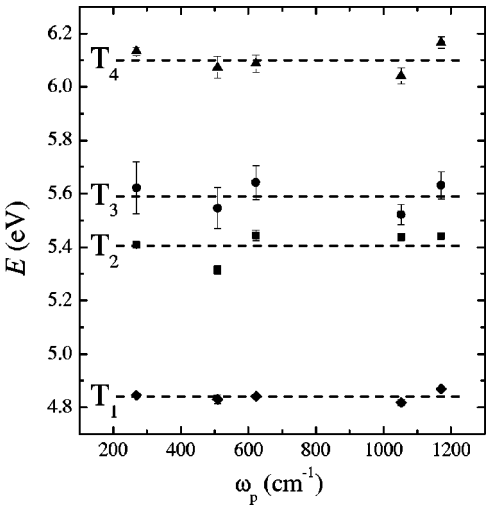

FIG. 7. CP interband transition energies vs plasmon frequency. The mean values for the transition energies are 4.84, 5.43, 5.59, and 6.10 eV, respectively.

Above a band-edge tailing region,[45] the absorption curves show a linear part, which is indicative of a direct band gap semiconductor. Furthermore, the absorption coefficient is on the order of several 10^4 cm^{-1} at energies about 0.5 eV above the effective band gap, again typical of a direct band gap semiconductor.

Figures 6(a) and 6(b) present the second derivates of the UV pseudodielectric function of sample C, which is representative of the entire sample set in that energy range. The

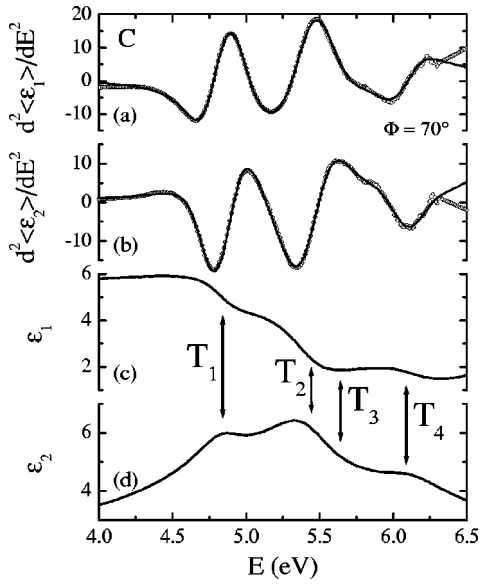

FIG. 6. (a, b) Second derivate of the pseudodielectric function of sample C, at 70° angle of incidence. Circles, experimental data; lines, MDF spectra described by four CP terms. (c, d) InN UV-dielectric function spectra of sample C, deduced from the SE data regression analysis. Three of the four transitions give rise to peak- or shoulder-like spectral features in ε_2. Arrows mark the CP transition energies T_1-T_4.

derivatives were calculated by locally fitting a third-order polynomial to the $\langle\varepsilon\rangle$ spectra using 35 data points centered around the spectral point of interest. The experimental data can be well described by four CP oscillators T_1-T_4 according to (3), whose positions are indicated by arrows. The exponents n_i were set to -0.5 for all CP oscillator terms corresponding to one-dimensional CP's and resulting in excellent description of the experimental data. It should be noted however that the dimensionality of the four CP's is in fact undeterminable here, since similar good data fits can be obtained assuming, e.g., $n_i=-1$ $(i=1,\ldots,4)$ corresponding to excitonic-type CP's, or a mixture of CP's with different dimensionalities. While the resulting CP energy parameters for the two lower energy transitions are affected only marginally by the choice of the CP dimensionality, the CP energy parameters for T_3 and T_4 are subject to changes of up to $\sim$0.2 eV when altering their n_i values.

The UV complex dielectric function of sample C derived from the SE data analysis accounting for surface roughness effects (see Sec. III) is plotted in Figs. 6(c) and (d). The main feature in the ε_2 spectrum is a doublet structure caused by the interband transitions T_1 and T_2 and peaking at 4.87 and 5.33 eV, the latter being the dominant one. On the high-energy side of this doublet, a shoulder is discernible around 6.10 eV linked to transition T_4. No spectral feature can be directly related to the faint and broad transition T_3, which however manifests itself clearly as an additional structure in the second derivate spectra depicted in Figs. 6(a) and 6(b). As shown in Fig. 7, none of the four interband transitions exhibits a significant dependence on the plasmon frequency. This is in accordance with our expectations, since the high-lying conduction bands involved in these transitions are supposed to be strongly depleted of free carriers.

The energy values of the CP oscillators and the respective features in the ε_2 spectrum, averaged over the sample set, are listed in Table II along with literature data. Very recently, empirical pseudopotential calculations based on a band gap

TABLE II. CP energy parameters and positions of corresponding features in the ε_2 spectrum between 4.0 and 6.5 eV. The values are averaged over the sample set studied. For comparison, previously reported theoretical and experimental data are given as well.

	Effective band gap energy (eV)	CP feature/parameter energy (eV)			
MDF CP energy E_i, this work[a]	0.65–0.80	4.84 (T_1)	5.41 (T_2)	5.59 (T_3)	6.10 (T_4)
ε_2 feature, this work[b]	<1	4.87	5.33[c]		6.05
Theory[d]	0.78 ($\Gamma_6-\Gamma_1$)	4.635 ($U_3-U_3, \sim 1/3\ L\rightarrow M$) 4.556 ($M_4-M_1$)	5.245 ($L_{2,4}-L_{1,3}$)	5.883 (H_3-H_3)	6.142 (M_2-M_1)
Theory[e]	~0.9	~4.6[c] ($L\rightarrow M$)	~5.1	~5.6	
Experiment[f]	<1	~5.0	~5.3[c]		
Experiment[g]	~2	4.85	5.55[c]		6.3
Experiment[h]	~2		5.3[c]		
Experiment[i]	1.9	4.9[c]	5.2		
Experiment[j]	2	4.7 4.95[c]	5.4		6.3

[a]Average value for all samples.
[b]Observed feature in experimental ε_2 spectrum.
[c]Main spectral feature in the range 4.0–6.5 eV.
[d]Fritsch *et al.* (Ref. 18), interband transition energies calculated by an empirical pseudopotential approach.
[e]Bechstedt *et al.* (Ref. 35), features in calculated ε_2 spectrum (*ab initio* method).
[f]Goldhahn *et al.* (Ref. 14), features in experimental ε_2 spectrum, obtained from SE studies on single-crystalline MBE-grown material.
[g]Sobolev and Zlobina (Ref. 46), energies of Lorentzian oscillators modeling the ε_2 spectrum calculated from experimental reflection data from Guo *et al.* (Ref. 7).
[h]Guo *et al.* (Ref. 47), features in ε_2 spectrum deduced from near-normal incidence reflection data on single-crystalline MOCVD-grown films.
[i]Wakahara *et al.* (Ref. 48), features in ε_2 spectrum deduced from near-normal incidence reflection data on MOCVD-grown crystalline material.
[j]Foley and Tansley (Ref. 50), features in $\varepsilon_{2,\perp}$ spectrum deduced from reflection data measured by Sobolev *et al.* (Ref. 49) on sputtered polycrystalline films.

energy of 0.59 eV for zinc-blende InN provided the electronic band structure for wurtzite-type InN with a fundamental band gap of 0.78 eV by exploiting the transferability of ionic model potential parameters between the two polytypes.[18] The interband transition energies that are derived from these calculations and closest match the CP transition energies observed by SE are given in Table II as well. According to this comparison, the doublet structure dominating the ε_2 spectrum is related to transitions at or close to the *L* point of the BZ. A similar doublet structure peaking at ~4.6 and ~5.1 eV with the low-energy component being the stronger one was predicted by recent *ab initio* calculations and also traced back to transitions along the *LM* line of the BZ.[35] The UV ε_2 dispersion observed by our SE measurements agrees fairly well with previous experimental ε_2 spectra taken from both low- and high-absorption edge material.[7,14,46–49] Recent SE data of Goldhahn *et al.* recorded on small-band-gap InN showed a principal doublet structure as well.[14] The main peak position at ~5.3 eV observed in their spectra is in excellent agreement with the dominating component of the doublet structure in our spectra at 5.33 eV. Interestingly, a pronounced spectral feature in the 5 eV range consisting of one to three components has even been observed for material exhibiting an effective band gap around 2 eV.[7,46–49] The relative strengths of these components however are partly different from our results.

According to the empirical pseudopotential calculations,[18] T_3 and T_4 in our spectra may be related to transitions at the *H* and *M* points of the BZ, respectively. Here, one has to keep in mind, however, the relatively large uncertainty of the T_3 and T_4 transition energies resulting from the unknown dimensionality of the corresponding CP's (see above) and a possible error source owing to the simplified isotropic data treatment. The *ab initio* calculations predicted a small feature in the ε_2 spectra at ~5.6 eV, i.e., close to transition T_3.[35] The ε_2 dispersion feature observed at 6.05 eV in our data and related to transition T_4 may have the same origin as features around 6.3 eV observed in ε_2 dispersions derived from re-

analyzed reflection data by Sobolev *et al.*[46] and deduced from near-normal incidence reflection data, respectively.[49,50]

V. SUMMARY

Employing spectroscopic ellipsometry from the mid-IR to the UV spectral range, the dielectric function of MBE-grown high-quality InN films with different free-electron properties was investigated. The onset of the absorption edge shifts from 0.65 eV for a free-carrier plasmon frequency ω_p of 268 cm^{-1} to 0.80 eV for $\omega_p = 1171$ cm^{-1}. No additional absorption was found near 1.9 eV, the formerly accepted band gap value. The UV dielectric function is dominated by a strong critical point structure at 5.41 eV likely related to electronic interband transitions at the *L* point of the Brillouin zone. Further transitions are located at 4.84, 5.59, and 6.10 eV.

ACKNOWLEDGMENTS

This work was partly supported by the EU project CLERMONT, the Wenner-Gren Foundation (Sweden), and the STINT Foundation (Sweden).

*Electronic address: aleka@ifm.liu.se

[1] V. Yu. Davydov, A. A. Klochikhin, R. P. Seisyan, V. V. Emtsev, S. V. Ivanov, F. Bechstedt, J. Furthmüller, H. Harima, A. V. Mudryi, J. Aderhold, O. Semchinova, and J. Graul, Phys. Status Solidi B **229**, R1 (2002).

[2] T. Matsuoka, H. Okamoto, M. Nakao, H. Harima, and E. Kurimoto, Appl. Phys. Lett. **81**, 1246 (2002).

[3] Y. Saito, H. Harima, E. Kurimoto, T. Yamaguchi, N. Teraguchi, A. Suzuki, T. Araki, and Y. Nanishi, Phys. Status Solidi B **234**, 796 (2002).

[4] A. G. Bhuiyan, A. Hashimoto, and A. Yamamoto, J. Appl. Phys. **94**, 2779 (2003).

[5] J. Wu, W. Walukiewicz, K. M. Yu, J. W. Ager III, E. E. Haller, H. Lu, W. J. Schaff, Y. Saito, and Y. Nanishi, Appl. Phys. Lett. **80**, 3967 (2002).

[6] T. L. Tansley and C. P. Foley, J. Appl. Phys. **59**, 3241 (1986).

[7] Q. Guo, O. Kato, M. Fujisawa, and A. Yoshida, Solid State Commun. **83**, 721 (1992).

[8] V. Yu. Davydov, A. A. Klochikhin, V. V. Emtsev, A. N. Smirnov, I. N. Goncharuk, A. V. Sakharov, D. A. Kurdyukov, M. V. Baidakova, V. A. Vekshin, S. V. Ivanov, J. Aderhold, J. Graul, A. Hashimoto, and A. Yamamoto, Phys. Status Solidi B **240**, 425 (2003).

[9] M. Yoshimoto, H. Yamamoto, W. Huang, H. Harima, J. Saraie, A. Chayahara, and Y. Horino, Appl. Phys. Lett. **83**, 3480 (2003).

[10] K. S. A. Butcher, M. Wintrebert-Fouquet Motlan, S. K. Shrestha, H. Timmers, K. E. Prince, and T. L. Tansley, Mater. Res. Soc. Symp. Proc. **743**, L11.23 (2003).

[11] T. V. Shubina, S. V. Ivanov, V. N. Jmerik, D. D. Solnyshkov, V. A. Vekshin, P. S. Kop'ev, A. Vasson, J. Leymarie, A. Kavokin, H. Amano, K. Shimono, A. Kasic, and B. Monemar, Phys. Rev. Lett. **92**, 117407 (2004).

[12] J. Wu, W. Walukiewicz, W. Shan, K. M. Yu, J. W. Ager III, E. E. Haller, H. Lu, and W. J. Schaff, Phys. Rev. B **66**, 201403 (2002).

[13] F. Li, D. Mo, C. B. Cao, Y. L. Zhang, H. L. W. Chan, and C. L. Choy, J. Mater. Sci.: Mater. Electron. **12**, 725 (2001).

[14] R. Goldhahn, S. Shokovets, V. Cimalla, L. Spiess, G. Ecke, O. Ambacher, J. Furthmüller, F. Bechstedt, H. Lu, and W. J. Schaff, Mater. Res. Soc. Symp. Proc. **743**, L5.9 (2003).

[15] A. Kasic, M. Schubert, Y. Saito, Y. Nanishi, and G. Wagner, Phys. Rev. B **65**, 115206 (2002).

[16] T. Inushima, M. Higashiwaki, and T. Matsui, Phys. Rev. B **68**, 235204 (2003).

[17] Z. G. Qian, W. Z. Shen, H. Ogawa, and Q. X. Guo, J. Appl. Phys. **92**, 3683 (2002).

[18] D. Fritsch, H. Schmidt, and M. Grundmann, Phys. Rev. B **69**, 165204 (2004).

[19] H. Lu, W. J. Schaff, J. Hwang, H. Wu, W. Yeo, A. Pharkya, and L. F. Eastman, Appl. Phys. Lett. **77**, 2548 (2000).

[20] H. Lu, W. J. Schaff, J. Hwang, H. Wu, G. Koley, and L. F. Eastman, Appl. Phys. Lett. **79**, 1489 (2001).

[21] H. Lu, W. J. Schaff, L. F. Eastman, J. Wu, W. Walukiewicz, D. C. Look, and R. J. Molnar, Mater. Res. Soc. Symp. Proc. **743**, L4.10 (2003).

[22] B. Arnaudov, T. Paskova, P. P. Paskov, B. Magnusson, E. Valcheva, B. Monemar, H. Lu, W. J. Schaff, H. Amano, and I. Akasaki, Phys. Rev. B **69**, 115216 (2004).

[23] A. Kasic, *Phonons, Free-carrier Properties, and Electronic Interband Transitions of Binary, Ternary, and Quaternary Group-III Nitride Layers Measured by Spectroscopic Ellipsometry* (Shaker, Aachen, 2003).

[24] R. M. A. Azzam and N. M. Bashara, *Ellipsometry and Polarized Light* (North-Holland, New York, 1989).

[25] H. G. Tompkins and W. A. McGahan, *Spectroscopic Ellipsometry and Reflectometry: A User's Guide* (Wiley, New York, 1999).

[26] A. Kasic, M. Schubert, S. Einfeldt, D. Hommel, and T. E. Tiwald, Phys. Rev. B **62**, 7365 (2000).

[27] A. A. Kukharskii, Solid State Commun. **13**, 1761 (1973).

[28] M. Schubert, T. E. Tiwald, and C. M. Herzinger, Phys. Rev. B **61**, 8187 (2000).

[29] M. Cardona, *Modulation Spectroscopy* (Academic, New York, 1969).

[30] S. Logothetidis, J. Petalas, M. Cardona, and T. D. Moustakas, Phys. Rev. B **50**, 18 017 (1994).

[31] S. Zollner, J. Appl. Phys. **90**, 515 (2001).

[32] J. W. Garland, H. Abad, M. Viccaro, and P. M. Raccah, Appl. Phys. Lett. **52**, 1176 (1988) showed that the proper functional representation for the optical dielectric function of GaAs and CdTe has partial Gaussian contribution. They further demonstrated that varying the exponent n_i in the Lorentzian representation of (3) effectively mimics the partial Gaussian broadening of the E_0 CP structure. In order to consider a possible partial Gaussian broadening of the CP feature of the dielectric function, the exponent n_0 was allowed to vary during the data regression analysis.

[33] A. Kasic, M. Schubert, B. Kuhn, F. Scholz, S. Einfeldt, and D. Hommel, J. Appl. Phys. **89**, 3720 (2001).

[34] By means of Hall-effect and high-resolution electron-energy-loss spectroscopy measurements an intrinsic electron accumulation layer was observed at the InN surface recently [H. Lu, W. J. Schaff, L. F. Eastman, and C. E. Stutz, Appl. Phys. Lett. **82**, 1736 (2003); I. Mahboob, T. D. Veal, C. F. McConville, H. Lu, and W. J. Schaff, Phys. Rev. Lett. **92**, 036804 (2004)]. For our samples, the sensitivity of the mid-IR SE data to such an accumulation layer is however too low to yield reliable results, and the plasmon frequency obtained by SE is understood as an average value over the entire film.

[35] F. Bechstedt, J. Furthmüller, M. Ferhat, L. K. Teles, L. M.R. Scolfaro, J. R. Leite, V. Yu. Davydov, O. Ambacher, and R. Goldhahn, Phys. Status Solidi A **195**, 628 (2003).

[36] H. Yao and C. H. Yan, J. Appl. Phys. **85**, 6717 (1999).

[37] S. Shokhovets, R. Goldhahn, G. Gobsch, S. Piekh, R. Lantier, A. Rizzi, V. Lebedev, and W. Richter, J. Appl. Phys. **94**, 307 (2003).

[38] A. Kasic, M. Schubert, T. Frey, U. Köhler, D. J. As, and C. M. Herzinger, Phys. Rev. B **65**, 184302 (2002).

[39] T. Inushima, T. Shiraishi, and V. Yu. Davydov, Solid State Commun. **110**, 491 (1999).

[40] J. S. Dyck, K. Kim, S. Limpijumnong, W. R. L. Lambrecht, K. Kas, and J. C. Angus, Solid State Commun. **114**, 355 (2000).

[41] V. Darakchieva, P. P. Paskov, E. Valcheva, T. Paskova, B. Monemar, M. Schubert, H. Lu, and W. J. Schaff, Appl. Phys. Lett. **84**, 3636 (2004).

[42] F. Agulló-Rueda, E. E. Mendez, B. Bojarczuk, and S. Guha, Solid State Commun. **115**, 19 (2000).

[43] Z. G. Qian, G. Yu, W. Z. Shen, H. Ogawa, and Q. X. Guo, Physica B **318**, 180 (2002).

[44] The IR-inactive $E_2{}^2$ phonon mode was observed by Raman scattering measurements within the range 491.6 and 492 cm^{-1} for samples A, B, and E, while for the films deposited on AlN without GaN buffer the $E_2{}^2$ mode is subjected to a blueshift to 490.4 cm^{-1} (sample C) and 490.3 cm^{-1} (sample D). The $E_2{}^2$ mode broadening values range from 4.2 to 7.3 cm^{-1}.

[45] The band-edge tailing is likely attributed to the carrier-phonon and the carrier-impurity interaction as well as structural disorder effects. See also, W. Z. Shen, L. F. Jiang, H. F. Yang, F. Y. Meng, H. Ogawa, and Q. X. Guo, Appl. Phys. Lett. **80**, 2063 (2002).

[46] V. V. Sobolev and M. A. Zlobina, Semiconductors **33**, 385 (1999).

[47] Q. Guo, H. Ogawa, and A. Yoshida, J. Electron Spectrosc. Relat. Phenom. **79**, 9 (1996).

[48] A. Wakahara, T. Tsuchiya, and A. Yoshida, Vacuum **41**, 1071 (1990).

[49] V. V. Sobolev, S. G. Kroituru, A. F. Andreeva, and V. Ya. Malakhov, Fiz. Tekh. Poluprovodn. (S. Peterburg) **13**, 823 (1979); Fiz. Tekh. Poluprovodn. (S.-Peterburg) **13**, 485 (1979).

[50] C. P. Foley and T. L. Tansley, Phys. Rev. B **33**, 1430 (1986).